Half-metallic complex perovskites Sr_2CrTO_6 as spintronics materials with high spin-polarization at room temperature

M. Musa Saad H.-E., A. Fiasal Elhag

[1] *Department of Physics, College of Science, Qassim University, Buraidah, 51452, Saudi Arabia*

Abstract:

Strong integration between spin-up or spin-down and charge of conduction electrons is a key in spintronics materials and devices. A few ferromagnetic (FM) or ferrimagnetic (FiM) transition metal complex perovskites have high spin-polarized (SP) conduction electrons at room temperature (RT), but it is formidable task to find other SP materials with high Curie temperature (T_C), and large magnetization suitable for spintronics applications. Here, we show that the complex perovskites Sr_2CrTO_6 (T = Mo, W, Re) have half-metallic (HM) nature with 100% spin-down-polarized conduction electrons, and FiM with T_C = 450 – 635 K. The coupling between the 3d, 4d or 5d transition metals (Cr – T) in Sr_2CrTO_6 (T = Mo, W, Re) lead to the high T_C, large saturation magnetization (m = 2.0, 2.0 and 1.0 μ_B), respectively, and HM electronic structure, in which only the spin-down bands cross the Fermi level, producing high SP (SP = -1) of the conduction electrons. It is believed that the complex perovskites Sr_2CrTO_6 could be synthesized experimentally and would prove useful for spintronics applications.

Keywords: Spintronics materials; Complex perovskite; Half-metallic; Ferrimagnetic

I. Introduction

Spintronics, or spin-transport electronics, is a modern technology in solid-state devices; exploiting both, the intrinsic spin of the electron and its associated magnetic moment in addition to its fundamental electronic charge. This technology came into view from basis discoveries concerning spin-dependent electron-transport phenomena in solid-state devices. In modern era, spintronics has developed as an approach that has revolutionized the market for electronic devices. Some predicted advantages of this new technology are the non-volatility of data storage, the increased speed of data processing, the high storage density, and the low energy consumption [1]. Spintronics devices like conventional electronic devices rely on the transport of electrical charge carriers in a semiconductor such as silicon. Currently, researchers trying to exploit the spin of the electron rather than its charge to create remarkable new generation of spintronics devices which will be smaller, more versatile and more robust than those presently making up silicon chips and circuit elements [2]. Spintronics device operates according to the simple scheme: (i) input data (information) is stored; written into spins as a particular spin orientation spin-up ($S_\uparrow$) or spin-down ($S_\downarrow$), (ii) the spins, being attached to mobile-electrons, carry the information along a conductor, and (iii) the output information is read at the terminal.

The manipulation of the electronic spin for information processing gives rise to many advantages and would open the way to novel applications. This field of spintronics has require to functional semiconducting, ferromagnetic (FM) or ferrimagnetic (FiM) materials at room temperature (RT). In that respect, several observations of room temperature FM or FiM in transition-metal complex perovskite materials have been reported [3-6]. Half-metallic (HM) complex perovskite condensed materials, which are metallic for one spin orientation, ($S_\uparrow$) or ($S_\downarrow$), while semiconductor or insulator for the opposite spin direction, ($S_\downarrow$) or ($S_\uparrow$). Moreover, the HM property is to be closely related to the giant magnetoresistance (GMR) phenomena observed in various complex perovskites, such as in Sr_2FeMoO_6 [7], A_2FeReO_6 (A=Ca, Ba) [8] and Sr_2CoMoO_6 [9].

HM materials with high spin-polarization (*SP*), preferably 100%, are promising for spintronics devices and have been searched enthusiastically. In order to develop spintronics technology, it is first necessary to, fully, explore potential materials and their properties; by obtaining a thorough understanding of spintronics phenomena we can effective utilize them to create spin-engineered materials and working devices. Here we present ab-initio investigations on the chromium-based complex perovskites Sr_2CrTO_6 with T 4d or 5d transition metal (T = Mo, W, Re). We optimize their structures fully and then investigate their stability, electronic structures and magnetic properties.

II. Theory and calculation methods

In this study, *ab-initio* self-consistent band structure calculations were performed using the all-electrons full potential linear muffin-tin orbital (FP-LMTO) method working within atomic plane wave expansion (PLW) [10]. In FP-LMTO method, the primitive cell with simple cubic symmetry is divided into non-overlapped atomic spheres and interstitial regions. Inside atomic muffin-tin spheres (MTSs), the charge density $\rho\,(r)$ is constructed from numerical solutions of radial Schrödinger's equations for each atom and the potential is represented via spherical harmonics expansions. In the interstitial region, the $\rho\,(r)$ is calculated from the Fourier transformations for LMTO orbitals [11] and the potential is expanded in plane waves. For all calculations, the plane-wave kinetic energy cut-off was 34.5 *Ry* (470 *eV*). Divisions of the Brillouin zone (BZ) along three directions for fast Fourier transform (FFT) [12] for the tetrahedron integration was sampled using 6×6×6, leading to at least 80 *k*-points in the irreducible part of the BZ. For the correct description of the wave functions in the interstitial region, maximal angular momentum *l* for expansion of the charge density and the potential in spherical harmonics, was inputted as $l_{max} = 6$ for Sr, M, T and O muffin-tin spheres (MTSs). The SP is unrestricted in the calculations, in order to account for both spin-up and spin-down. Single ($\kappa = 2$) for *spdf* LMTO basis was used, each radial function inside the spheres is matched to the Hankel function in the interstitial region, for describing the valence bands. The radius of the MTS for each atom is taken as different so that the sphere do not overlap, thus, for each compound, the MTs radii change with the phase. Moreover, the employ of the FP-LMTO ensures that the calculation is independent of the option of MTSs radii. It has been established that the *fcc* crystal-structures are close enough, that no empty sphere (ES) is needed to insert in the unit cells [4,13].

The spin-dependent total and partial densities of states (DOSs) for Sr_2CrTO_6 were obtained from the local spin density approximation plus correlation energy (LSDA+*U*), resolving spin-up and spin-down states in the calculations. In order to obtain better results of DOSs, the correlation parameters, Coulomb repulsion (*U*) and Hund's rule exchange (*J*) [14,15], were utilized for correlated *d*-electrons. For 3d, 4d and 5d electrons, only three effective Slater integrals F^0, F^2 and F^4 (in *Ry* units; $eV \approx 0.0735$ *Ry*) require being determined for FP-LMTO [13]. The Hubbard parameters ($U = 3.0 – 5.0$ *eV*, $J = 0.89$ *eV*) and ($U = 1.0$ *eV*, $J = 0.89$ *eV*) are used for the strongly M (3*d*) and weakly T (4*d*/5*d*) correlated states, respectively [16,17]. Accordingly, the input of Slater values are; $F^0 = 0.2940 – 0.3675$ *Ry*, $F^2 = 0.5636$ *Ry* and $F^4 = 0.3522$ *Ry* for 3*d*-states while $F^0 = 0.07350$ *Ry*, $F^2 = 0.5636$ *Ry* and $F^4 = 0.3522$ *Ry* for 4*d*/5*d*-states.

III. Results and discussion

3.1. Crystal structures of Sr_2CrTO_6

The family of complex perovskite is probably the most extensively studied family of inorganic oxides. The interest in compounds belonging to this family arises in the large and ever surprising variety of physical, chemical and engineering properties exhibited and the flexibility to accommodate almost all of the elements in the periodic system, expect Noble gas ones. The crystal structure of the complex perovskite A_2MTO_6 is known to be very flexible and the A, M and T ions can be varied leading to the large number of known compounds with complex perovskite or related structures. Most complex perovskites are distorted and do not have the ideal cubic structure; three major factors are identified as being responsible for the distortion: (i) size effects, (ii) deviations from the ideal composition and (iii) the Jahn-Teller effect. It is rare that a distortion of a certain complex perovskite compound can be assigned to a single effect; in most cases, several factors act on the crystal structure. The relevance of size effect, pioneering work on the structure of simple perovskite AMO_3, was conducted by Goldschmidt that formed the basis for further exploration of perovskites [18]. In ideal cubic case, the cell axis *a* geometrically relates to the ionic radii, r_A, r_M, r_T, and r_O in A_2MTO_6, as described in:

$$a = \sqrt{2}\left(r_A + r_O\right) \;\; = \;\; 2\left(\frac{r_M + r_T}{2} + r_O\right) \qquad (1)$$

The ratio of the two expressions to the cell length in Eq. (1) is called Goldschmidt's tolerance factor (*t*) and allows us to estimate the degree of distortion [19]. It is based on ionic radii i.e. purely ionic bonding is assumed, but can be regarded as an indication for A_2MTO_6 with a high degree of ionic bonding; can be described as:

$$t \;\; = \;\; \frac{1}{\sqrt{2}}\frac{\left(r_A + r_O\right)}{\left(\frac{r_M + r_T}{2} + r_O\right)} \qquad (2)$$

The ideal cubic complex perovskite has ($t \approx 1.00$), otherwise, if the A-ion is smaller or M and/or T ions are larger than the ideal values then *t* becomes smaller than 1. As a result, the MO_6 octahedra will tilt in order to fill the space. However, the cubic crystal structure occurs if ($0.99 < t < 1.05$) [19,20]. Lower values of *t* will lower the symmetry of the crystal structure; cubic becomes rhombohedral or orthorhombic. For example, the distorted Ca_2CrSbO_6 with ($t = 0.88$) is monoclinic (P2$_1$/n space group) [21], and for Ca_2FeReO_6, as well, due to the low

tolerance factor ($t = 0.89$) a monoclinic unit cell is expected [22]. On the other hand, if t is larger than 1.0 due to a large A or small M and/or T ions then hexagonal variants of structure are stable, as in Ba_2FeReO_6 [23].

The main types of deviation from the cubic complex perovskite can be sum up into four categories: (i) displacement of M-cation from the center of the octahedra, (ii) displacement of A-cation from the cavity center, (iii) distortion of octahedral cage and/or (iv) tilting of octahedra, where tilting of the octahedra is definitely the most common form. Tilting of the octahedra can be described by using the Glazer tilt system (GTS) developed by A. M. Glazer [19,24]. The GTS describes the tilt system by rotations of MO_6/TO_6 octahedra about the three axes of the unit cell *abc*. The tilting of the octahedra reduces the symmetry of the undistorted complex perovskite tilt-system ($a^0a^0a^0$), where the GTS assigned to Fm-3m space group is $a^0a^0a^0$ (No. 23) [19]. In addition, the stability of crystal composition with different atoms, symmetry, tilt-systems and structure can be evaluated by comparing the global instability index (GII) [19,25]. The GII value is typically < 0.1 v.u., valence units, for unstrained structures and as large as 0.2 v.u. in a structure with lattice-induced strains [19].

For complex perovskites Sr_2CrTO_6 (T = Mo, W, Re), it verified that they have been stabled in the face-centered cubic (*fcc*) structure with space group of Fm-3m (No. 225) in ($a^0a^0a^0$) GTS (No. 23). As well as their tolerance factor are calculated and found to be around the unity ($t \approx 1.0$) and have small global instability indexes, GII < 0.10, as showed in Tables 1 and 2. The structural information are obtained using SPuDS (Structure Prediction Diagnostic Software) [19,26]. At room temperature (RT), the tolerance factors (*t*), lattice parameters (*a*), unit cell volumes (*V*), oxygen positions O (u), and bond-lengths have been calculated and summarized in Tables 1, 2 and 3, in comparison to the available values in the literature. The general atomic positions in Sr_2CrTO_6 unit cells are used according to the *fcc* (Fm-3m) crystallographic, see Table 3. The oxygen position u depends on the choice of T (4d/5d) site, as revealed in Table 2.

Table 1. Crystal ionic radii of Cr and T ions (in Å) in high-spin state, the ionic radius of Sr^{2+} is 1.58 Å and of O^{2-} is 1.32 Å [47]. The tolerance factors calculated using Eq. (2), for Sr_2CrTO_6.

Compound	Cr^{3+}	T			t
		Mo^{5+}	$W^{5+ a}$	Re^{5+}	
Sr_2CrMoO_6	0.615	0.610 [a]	-	-	0.9944 [b]
Sr_2CrWO_6	0.615	-	0.620 [a]	-	0.9987 [c]
Sr_2CrReO_6	0.615 [d]	-	-	0.520	1.0064

* *a* Ref. [28], *b* Ref. [20] , *c* Ref. [29], *d* Refs. [30,31]

Table 2. Lattice parameters, unit-cell volumes, bond-valence sums, and global instability indexes (GII) for Sr_2CrTO_6 (T = Mo, W, Re) in the ($a^0a^0a^0$) Glazer tilt system, (No. 23).

Compound	a (Å)	V (Å³)	Bond-valence sum (v.u.)				GII
			Sr	Cr	T	O	
$SrCrMoO_6$	7.9098 [a]	494.885	1.9174	3.0000	5.0000	1.9725	0.04265
Sr_2CrWO_6	7.8758 [b]	488.531	1.9806	3.0000	5.0000	1.9935	0.01001
Sr_2CrReO_6	7.8158 [c]	477.450	2.0969	3.0000	5.0000	2.0323	0.05004

* *a* Ref. [20], *b* Ref. [32] , *c* Ref. [33],

Table 3. The main interatomic bond-lengths in Sr_2CrTO_6, calculated at 298 K.

Compound	Bond-length (Å)		
	Sr – O ×12	Cr – O ×6	T – O ×6
$SrCrMoO_6$	2.7966	1.9805	1.9745
Sr_2CrWO_6	2.7846	1.9805	1.9575
Sr_2CrReO_6	2.7634	1.9805	1.9275

**Table 4.** Atomic -sites and -positions for Sr_2CrTO_6 in the *fcc* unit cells at RT. The oxygen position O (u) depends mainly on the choice of T (4d/5d) in each compound.

Compound	Sr_2CrTO_6		
T (4d/5d)-site	**Mo**	**W**	**Re**
Sr 8c (x, y, z)	(¼,¼,¼)	(¼,¼,¼)	(¼,¼,¼)
Cr 4a (x, y, z)	(0,0,0)	(0,0,0)	(0,0,0)
T 4b (x, y, z)	(½,½,½)	(½,½,½)	(½,½,½)
O 24e (x, y, z)	(u, 0, 0)	(u, 0, 0)	(u, 0, 0)
u	0.2504	0.2515	0.2534

3.2. Electronic and magnetic properties of Sr_2CrTO_6

Calculations of total and partial density of states (DOS) as a function of energy (E) for each complex perovskite Sr_2CrTO_6 (T = Mo, W, Re) have been performed by using the correlated LSDA+U method. During the study, it has been found that ferromagnetic (FM) phase converges to ferrimagnetic (FiM) phase for all considered structures; FiM phase is more stable than the FM phase. It is found that the total energy of FiM phase is lower than that of the FM phase in Sr_2CrTO_6. The FiM magnetic phases materialize the spin magnetic configurations of the two energetic ions, Cr (3d) and T (4d/5d), in Sr_2CrTO_6. Consequently, only the DOSs from cubic and FiM structures are presented. This result is in agreement with theoretical conclusion that the ground state of these systems are in FiM structure [20,34-37]. The DOS results, for spin-up (upper curve; +DOS) and spin-down (lower curve; –DOS) per unit cell are plotted in DOS figures. The horizontal axis stands for the energy relative to the Fermi energy (Energy (eV)), so the Fermi level was situated at (E_F = 0.0 eV). In order to understand in some more detail the origin of the electronic and magnetic properties of Sr_2CrTO_6 (T = Mo, W, Re), we critically examine the partial electronic density of states (PDOS) of these systems. The basic critical ingredients in the total density of states (TDOS) are the energetic *d*-states of the Cr (3d) and T (4d/5d) transition metals, which in turn are split into t_{2g} and e_g states by the octahedral crystal field (OCF) produced by the oxygen octahedra Cr (3d)–O_6 and T(4d/5d)–O_6. The t_{2g} states having lower energy and place for three electrons per spin channel, whereas the e_g states are higher in energy and have place for two electrons per spin channel. Furthermore, due to the exchange splitting, t_{2g} bands degenerate into double orbitals (d_{xz}, d_{yz}) and one singlet orbital (d_{xy}), while e_g bands degenerate into two singlet orbitals (d_{x2-y2}, d_{z2}), these seen in Figs.3, 5 and 7, which shows the partial densities of states of t_{2g}, e_g and 2p orbitals in Sr_2CrTO_6.

Fig. 1 illustrates the assembled TDOSs, from the TDOSs close to the E_F in the panels, it is observed a half-metallic (HM) character in all complex perovskites Sr_2CrTO_6 (T = Mo, W, Re) with high spin-polarization of conduction-band. Since the spin-down evidences a conductor feature, there are states crossing E_F, while the spin-up channels indicate insulator behavior with energy-gaps in TDOSs↑. The values of energy-gaps in spin-up are calculated and found to be E_g = 2.25 eV for T = Mo, E_g = 2.66 eV for T = W and E_g = 2.17 eV for T = Re.
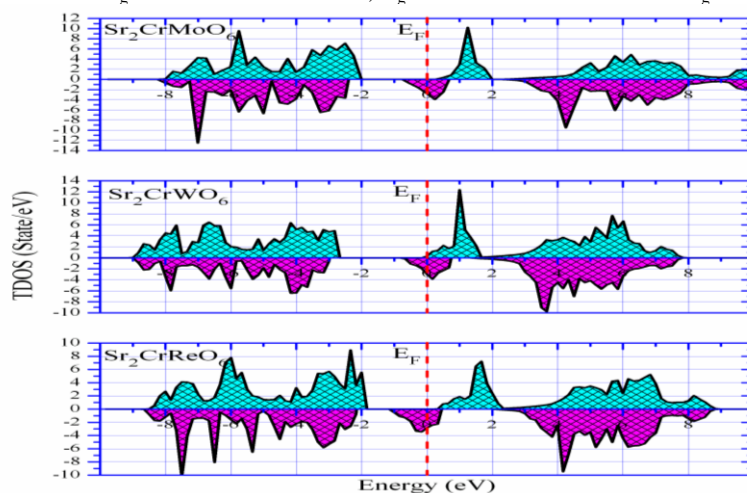
Fig. 1. The spin-up and spin-down TDOSs of Sr_2CrTO_6 (T = Mo, W and Re).

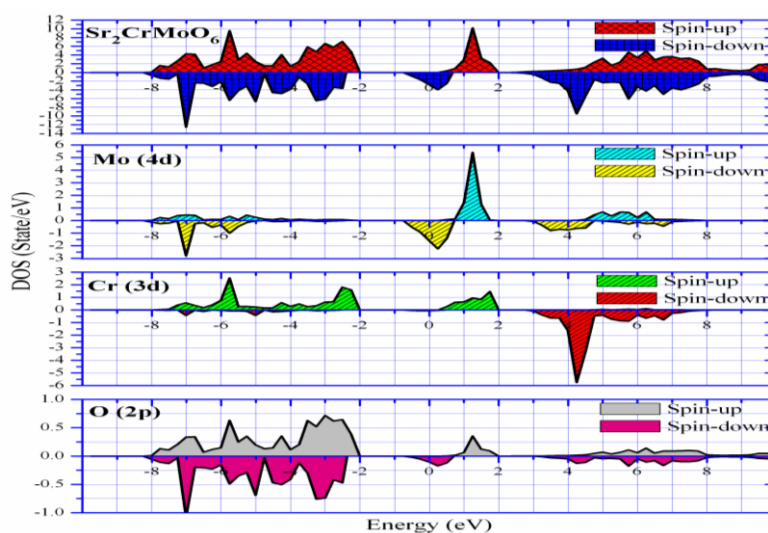### 3.2.1. Sr$_2$CrMoO$_6$

For Sr$_2$CrMoO$_6$, Fig. 2 shows the calculated TDOS and various projected PDOSs from the spin-polarized LSDA+U calculations. The calculations for the perfect structure give the ground state to be of HM character with a finite DOS in the spin-down channel and a zero DOS in the spin-up channel with an energy-gap through E$_F$ of about 2.25 eV, and antiferromagnetic ordering between the high spin Cr^{3+} (3d^{3+}) and Mo^{5+} (4d^{1+}) ions. For our discussion of DOS, which is limited to an energy window of −10 eV to +10 eV, we are primary concerned with the energetic states in Sr$_2$CrMoO$_6$; Cr (3d), Mo (4d) and O (2p), since the Sr (5s) inactive states appear at higher energy. It clearly seen that the Mo (4d)-t$_{2g}$↓ states are responsible for the conductivity feature; the Mo (4d) bands in the spin-down configuration shows that the energy spans from the -2.00 eV to 0.25 eV. In addition to, the conduction band is mainly composed of Mo (4d) character, which hybridizes with the O (2p) states and a tiny Cr (3d) character. The presence of a cubic symmetry of the octahedral coordination of the O atoms around the Cr and Mo sites results into triply degenerate t$_{2g}$ orbitals with high energy. The E$_F$ lies in the gap between the Cr (3d)-t$_{2g}$↑ and Cr (3d)-e$_g$↑ sub-bands, as shown in Fig. 3. The spin-down conduction band crossing E$_F$ is dominated by the Mo (4d)-t$_{2g}$↓ and O (2p)↓ states while the Cr (3d)-t$_{2g}$↓ states have a smaller contribution.

On the other hand, the spin-up band in the valence region, from -8 eV to -2 eV, is mostly of the Cr (3d)-t$_{2g}$↑ and O (2p)↑ states, without any appreciable Mo (4d)-t$_{2g}$↑ or Mo (4d)-e$_g$↑ contribution. While a sharp narrow in spin-up band just above E$_F$ is mostly of the Mo (4d)-t$_{2g}$↑ and Cr (3d)-e$_g$↑ states from +0.5 eV to +2 eV. Consequently, the 180° antiferromagnetic superexchange interaction mechanism of the long range Cr (3d)-t$_{2g}$↑ – O (2p$_\pi$) – Mo (4d)-t$_{2g}$↓ is responsible for the HM behavior in Sr$_2$CrMoO$_6$. The total and partial spin magnetic moments are calculated using LSDA and LSDA+U schemes, as seen in Table 5, at Cr (3d^3; t$_{2g}$^{3}, S = 3/2) are 2.192 and 2.902 μ_B and at Mo (4d^1; t$_{2g}$^{1}, S = 1/2) are -0.322 and -0.784 μ_B, respectively. Yield ferrimagnetic (FiM) spin coupling with total magnetic moments per unit cell of 1.926 and 2.017 μ_B. These characteristics are comparable with those recently reported from GGA and GGA+U calculations and experimental measurement values.

Table 5. The partial and total magnetic moments information for the perfect Sr$_2$CrMoO$_6$, calculated using LSDA and LSDA+U compare with GGA and GGA+U results from Refs. [20,34,35] and experimental measurements from Refs. [36,37].

Method	m_{Cr} (μ_B)	m_{Mo} (μ_B)	m_O (μ_B)	m_T (μ_B/f.u.)
LSDA	2.192	-0.322	-0.065	1.926
LSDA+U	2.902	-0.784	-0.092	2.017
GGA	2.285 [a]	-0.435	-	2.00
GGA+U	2.882	-0.636	-	2.00
Exp.	2.557 [b]	-0.330 [c]	-	2.00 [d]

Fig. 2. TDOS of Sr$_2$CrMoO$_6$ and Cr (3d), Mo (4d), O (2p) projected PDOSs, for spin-up and spin-down states.
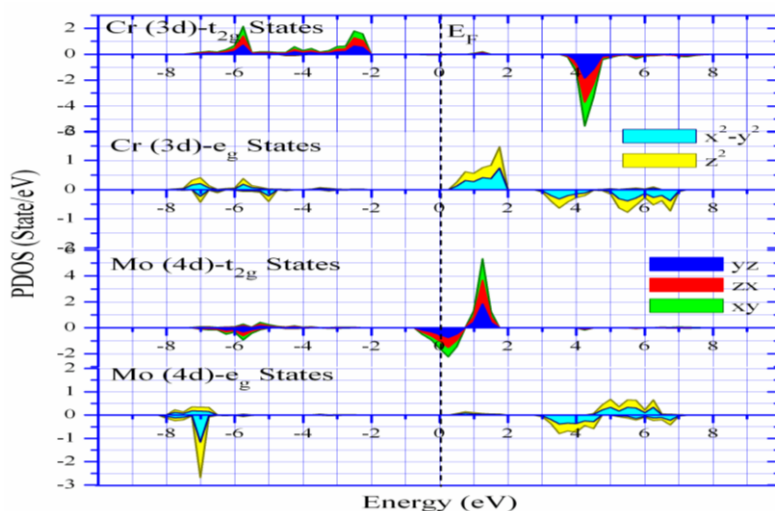
Fig. 3. Spin-up and spin-down PDOSs of Cr (3d)-t_{2g}, Cr (3d)-e_g, Mo (4d)-t_{2g} and Mo (4d)-e_g in Sr_2CrMoO_6.

3.2.2. Sr_2CrWO_6

Fig. 4 illustrates the TDOS and PDOSs of the perfect Sr_2CrWO_6 complex perovskite from LSDA+U calculations. The obtained results are agreement with previous LSDA+U calculations [32,38]. In TDOS↑, there is an energy-gap of about 2.66 eV between the occupied Cr (3d) and unoccupied W (5d) partial bands. Since the energy-gap in the spin-up produces from the antiferromagnetic coupling between Cr (3d) and W (5d) states, this situation emerges as peaks of 3d and 5d bands polarized antiferromagnetically demonstrate the Cr (3d) ↑ and W (5d) ↓ form. Therefore, the spin-up electrons are insulating while the spin-down electrons are metallic with bandwidth of 1.67 eV, resulting in full (100%) spin-polarized of the conduction electrons at E_F. For that reason, Sr_2CrWO_6 materials allow electrons of spin-down direction to move through them as though they were passing through a normal metal, while blocking electrons of the spin-up. As seen in Fig. 4, the conduction band in spin-down orientation is attributed mainly to the contribution of W (5d) ions with tiny contribution of Cr (3d). Therefore, the DOS of Sr_2CrWO_6 show an energy-gap at E_F in the spin-up direction typical for half-metallic ferrimagnetism (HM-FiM). From the PDOSs in Fig.5, the three-fold degenerate Cr t_{2g} states of the spin-up channel are filled Cr^{3+} ($3d^3$: t_{2g}^3↑); consequently the d_{xy}↑, d_{xz}↑ and d_{yz}↑ orbitals are at the energy range -8 eV ~ -2 eV in the valance bands. Therefore, the E_F ends up in the OCF gap of $\Delta_o \approx 2.32$ eV between Cr (3d)-t_{2g} and Cr (3d)-e_g states. Due to the antiferromagnetic coupling in Cr (3d) – W (5d) pair, the spin-down channel in W (5d) is occupied by one electron; it contains one electron in t_{2g} states W^{5+} ($5d^1$: t_{2g}^1↓). This means that the W (5d)-t_{2g}↓ states are only filled to about one-two, resulting in high DOS of d_{xy}↓ and d_{yz}↓ at E_F in spin-down channel. Furthermore, due to hybridization between states in Sr_2CrWO_6, Cr (3d)-t_{2g}↓ states achieved small occupation, while W (5d)-t_{2g}↑ states in the spin-up channel are essentially empty; hybridization with Cr (3d)-t_{2g}↑ states results nevertheless in a finite, small occupation above E_F. In addition to, the magnetic structure in Sr_2CrWO_6 can be assign to the antiferromagnetic superexchange interactions between Cr (3d) and W (5d) via intermediated oxygen atoms in the 180° long-chain Cr (3d-t_{2g}↑) – O ($2p_\pi$) – W (5d-t_{2g}↓). This superexchange between Cr (3d) and W (5d) states leads to FiM ordering below Curie temperature $T_C \approx 458$ K. The calculated spin magnetic moments from LSDA and LSDA+U method for Sr_2CrWO_6 are; 2.226 and 2.990 μ_B for Cr (3d), -0.3221 and -0.662 μ_B for W (5d) with a total magnetic moment of 1.937 and 2.172 μ_B, which are 94% agreement to the GGA and GGA+U results [38,39], see Table 6.

Table 6. The partial and total magnetic moments information for the perfect Sr_2CrWO_6, calculated using LSDA and LSDA+U compare with GGA and GGA+U results from Refs. [38,40] and experimental measurements from Refs. [32,40,41].

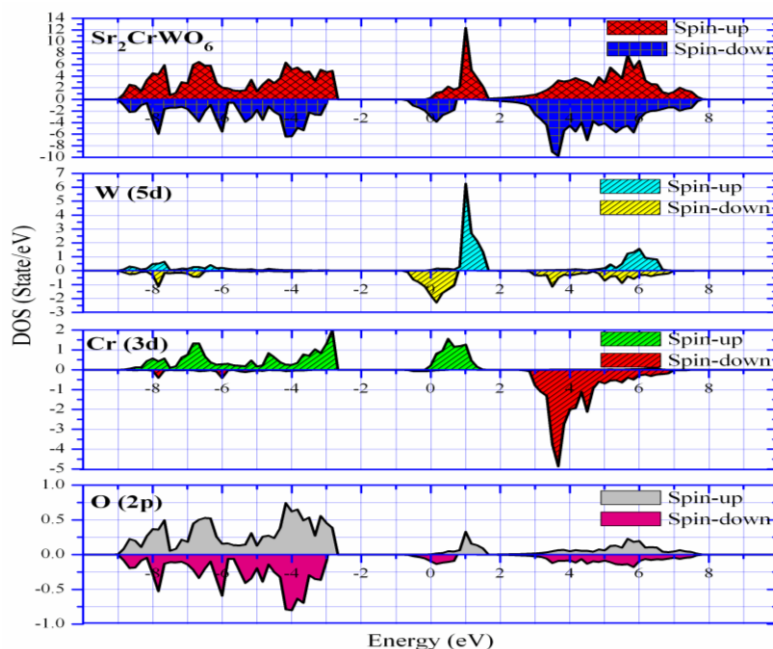| Method	m_{Cr} (μ_B)	m_W (μ_B)	m_O (μ_B)	m_T (μ_B/f.u.)
LSDA	2.226	-0.321	-0.068	1.937
LSDA+U	2.990	-0.662	-0.112	2.172
GGA	2.285 [a]	-0.435	-	2.00
GGA+U	2.882	-0.636	-	2.00
Exp.	2.557	-0.330	-	2.00

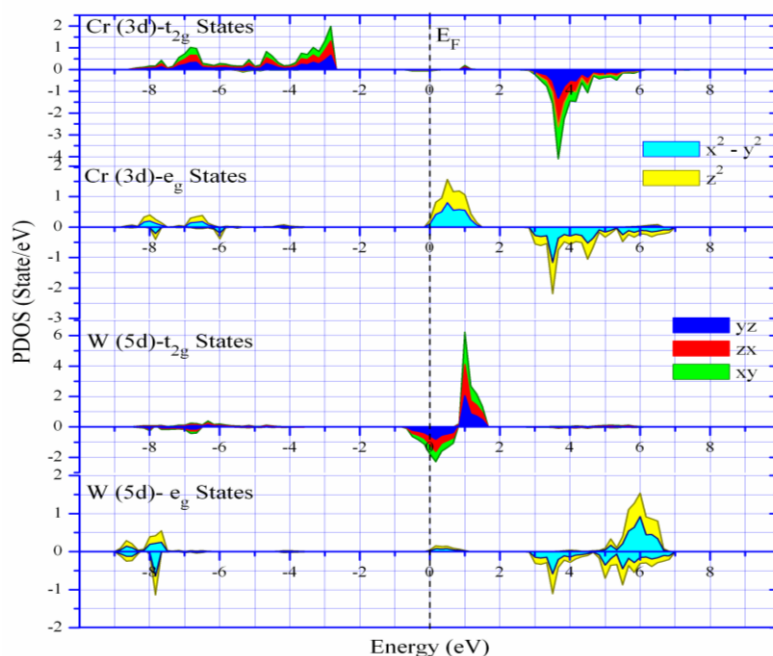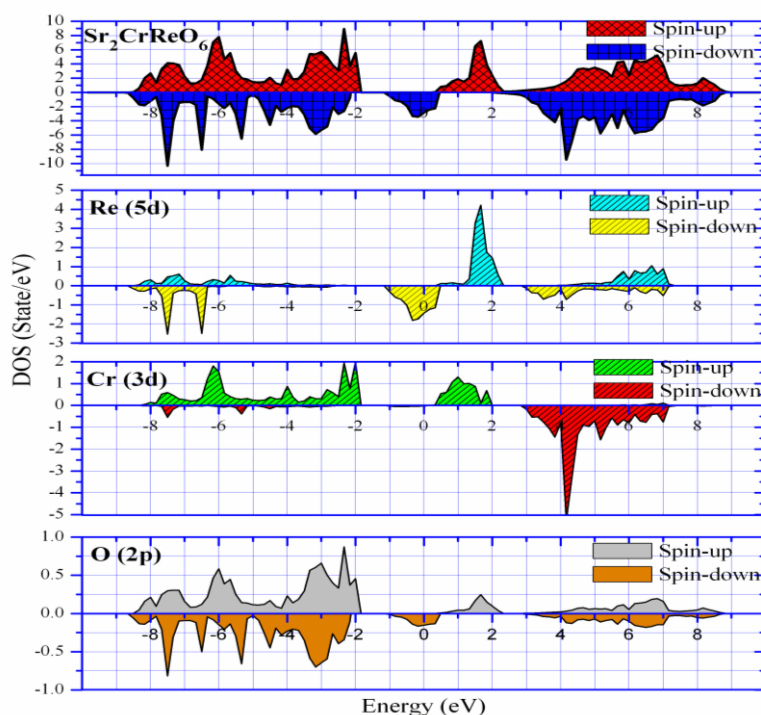**Fig. 4.** TDOS of Sr_2CrWO_6 and Cr (3d), W (5d), O (2p) projected PDOSs, for spin-up and spin-down states.

Fig. 5. Spin-up and spin-down PDOSs of Cr (3d)-t_{2g}, Cr (3d)-e_g, W (5d)-t_{2g} and W (5d)-e_g in Sr_2CrWO_6.

3.2.3. Sr_2CrReO_6

The calculated TDOS and PDOSs for the third member Sr_2CrReO_6 are given in Figs. 6 and 7. From the TDOS in the upper panel in Fig. 6, one can clearly see that the Re-based compound Sr_2CrReO_6 has HM nature. The energy-gap in the spin-up channel is around 2.16 eV. The energy-gap between the occupied bands is observed in spin-up of TDOS, while a finite band in spin-down of TDOS expanded from -1.17 to 0.50 eV. Similarly as in Sr_2CrWO_6, the E_F in Sr_2CrReO_6 falls just where the Cr 3d spin-up band is split due to the OCF, whereas in the spin-down channel there is a considerable hybridization of Cr (3d) with Re (5d) states at E_F.

Table 7. The partial and total magnetic moments information for the perfect Sr_2CrReO_6, calculated using LSDA and LSDA+U compare with GGA and GGA+U results from Refs. [38,39,44] and experimental measurements from Ref. [42].

Method	m_{Cr} (μ_B)	m_{Re} (μ_B)	m_O (μ_B)	m_T (μ_B/f.u.)
LSDA	2.131	-0.910	-0.140	1.041
LSDA+U	2.916	-1.467	-0.288	1.092
GGA	-	-	-	-
GGA+U	2.423	-1.272	-0.151	1.00
Exp.	2.521	-0.221	-	1.00

Fig. 6. TDOS of Sr_2CrReO_6 and Cr (3d), Re (5d), O (2p) projected PDOSs, for spin-up and spin-down states.

The spin-resolved TDOS and PDOSs for Sr_2CrReO_6 are shown in Figs. 6 and 7. The OCF splitting between t_{2g}−e_g states is larger than the exchange splitting between t_{2g}− t_{2g} states, suggesting the low spin state of Re (5d). In TDOS↑, the band extends from −8.67 to −1.83 eV below the E_F is composed mainly of O (2p) and Re (5d) states, and Cr (3d) has also some contribution in −8.0 to −1.5 eV. The band whose main contribution is Cr (3d)-t_{2g} states is localized between the O (2p) bands. The sharp narrow band just above the E_F is mostly of Re (5d)-t_{2g} states origin, between 1.0 and 2.0 eV, Cr (3d)-e_g has also some contribution in this region. In TDOS↓, like the spin-up band, the band from −8.67 to −1.83 eV is composed mainly by O (2p) and Re (5d) states. The band from −1.5 – 0.5 eV is contributed mainly by the Re (5d)-t_{2g} states. The total spin magnetic moment is 1.0 μ_B, which comes mostly from Cr (3d) and Re (5d) ions. The Cr (3d) states are mainly t_{2g}^3 spin-up electrons, which corresponding to the ionic valence of Cr^{3+}. Ignoring the extended d states between −8.5 and −2.5 eV, which are hybridized bonding states with O (2p) states, the Re (5d) is t_{2g}^2 spin-down state. Therefore, in the ground state, the molecular formula may be $Sr_2^{2+}Cr^{3+}Re^{5+}O_6^{2-}$. The magnetic spin states of Re (5d) (S = 1) couples antiferromagnetically to the high spin states of Cr (3d) (S = 3/2), resulting HM-FiM ground state. From Table 7, the LSDA and LSDA+U spin magnetic moments for Sr_2CrReO_6 are; 2.131 and 2.916 μ_B for Cr (3d), -0.91 and -1.467 μ_B for Re (5d) and total magnetic moment of 1.041 and 1.092 μ_B, respectively, which are agreement to the GGA and GGA+U results [42,43].
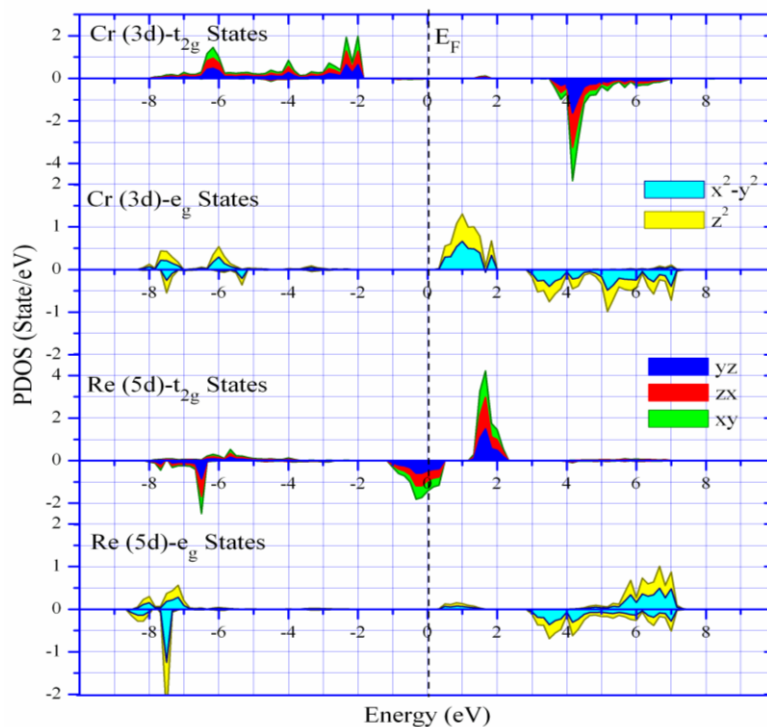
**Fig. 7.** Spin-up and spin-down PDOSs of Cr (3d)-t_{2g}, Cr (3d)-e_g, Re (5d)-t_{2g} and Re (5d)-e_g in Sr_2CrReO_6.

IV. Conclusions

A systematic structural, electronic and magnetic structures investigation of the chromium-based complex perovskites Sr_2CrTO_6 (T = Mo, W, Re) have been performed by employing LSDA and LSDA+U calculations. It is demonstrated that the HM character in Sr_2CrTO_6 is not caused by the indirect long range Cr – O – T pdd-$_\pi$ couplings that are simultaneously responsible for the FiM character. The calculated level distributions and spin magnetic moments indicate the Cr^{3+} and T^{5+} states, in terms of which all the itinerant FiM state in Sr_2CrTO_6. The population analyses show that Sr_2CrTO_6 have nearly the same valence state combinations due to strong intrinsic pd covalency effects, which accounts for the similar O (2p) – T (4d/5d) spectral structures observed in them. The main difference between $Sr_2Cr(Mo,W)O_6$ and Sr_2CrReO_6 is that Mo^{5+}/W^{5+} ($4d^1/5d^1$) has one electron less than Re^{5+} ($5d^2$), causing the Mo/W (4d/5d)-t_{2g} states to shift upwards in energy, away from the E_F. As a result, the hybridization at the energy-gap becomes less pronounced, and the energy-gap is preserved. The conduction bands in spin-down orientation are attributed mainly to the contributions of Mo (4d), W (5d) and Re (5d) states with tiny contributions of Cr (3d). Moreover, the chromium-based complex perovskites Sr_2CrTO_6 are found to be HM-FiM, with 100% spin-down polarization ($SP = -1$) and highest Curie temperature $T_C = 450 – 635$ K, see Table 8. In search of complex perovskites with high T_C, we noticed an intriguing trend (Fig.8) in the measured T_C with the total number of valence electrons (N_V) of the transition metals in Cr – T ions. To emphasize the observed trends we included the T_C for the 5d complex perovskites, Sr_2CrTaO_6, Sr_2CrOsO_6 and Sr_2CrIrO_6, which, however, will not be further considered here.

Table 8. The stable types, total number of valence electrons (N_V) in Cr^{3+} – T^{5+} ions, the partial, total, theoretical ($m^{Th.}$) and calculated ($m^{Cal.}$) from LSDA+U of spin magnetic moments, and the Curie temperatures (T_C).

Compound	N_V	Type	$m^{Th.}$	$m^{Cal.}$	m_{Cr}	m_T	m_O	T_C
Sr_2CrMoO_6	4	HM-FiM	2.0	2.017	2.251	-0.357	-0.106	450 [a]
Sr_2CrWO_6	4	HM-FiM	2.0	2.172	2.557	-0.439	-0.082	458 [b]
Sr_2CrReO_6	5	HM-FiM	1.0	1.092	2.423	-1.272	-0.504	635 [c]

*** *a* from Refs. [4,35], *b* from Ref. [40], *c* from Refs. [40,41].
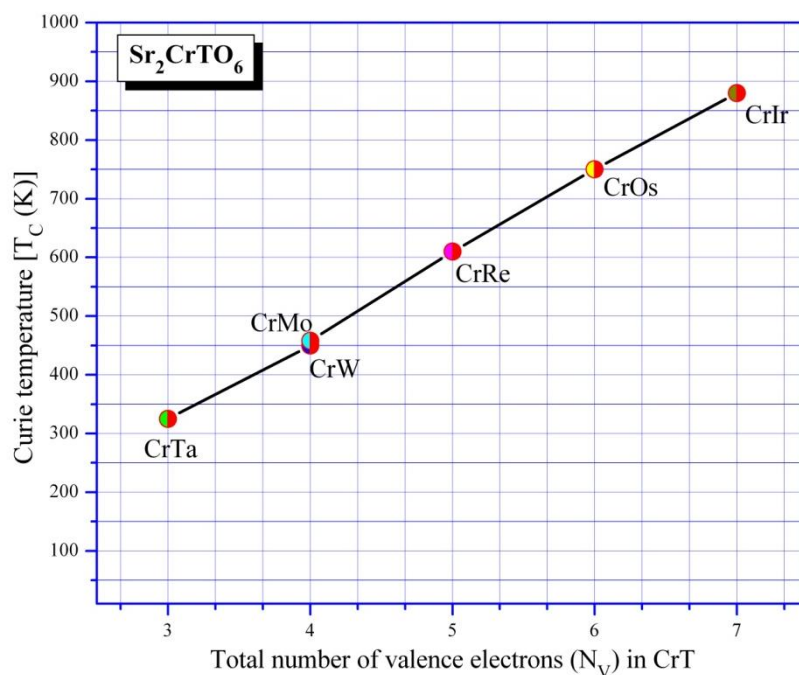
Fig. 8. Calculated Curie temperature (T_C) as a function of total number of valence electrons (N_V) in Cr (3d)–T (4d/5d) energetic pairs in complex perovskites Sr_2CrTO_6 (T = Mo, W and Re), we added CrTa, CrOs and CrIr, from Refs. [4,40], to complete the picture of 3d-5d pairs.

References
[1]   R. Jansen, S. P. Dash, S. Sharma, B. C. Min, Semicond. Sci. Technol. 27, 083001, (2012).
[2]   Nikita V. Volkov, Phys.-Usp. 55, 250, (2012).
[3]   Kobayashi K.-I., Kimura T., Sawada H., Terakura K., Tokura Y., Nature, V. 395, Issue 6703, (1998), 677.
[4]   D Serrate, J M De Teresa, M R Ibarra, J. Phys.: Condens. Matter 19, 023201, (2007).
[5]   O. Navarro, B. Aguilar, M. Avgnon, J. Magn. Magn. Mater. 322, 9-12, (2010), 1246.
[6]   Si-Da Li, Peng Chen, Bang-Gui Liu, AIP Advances 3, 012107, (2013).
[7]   D.D. Sarma, P. Mahadeva, T. Saha-Dasgupta, S. Ray, A. Kumar, Phys. Rev. Lett. 85, (2000), 2549.
[8]   W. Prellier, V. Smolyaninova, Amlan Biswas, C. Galley, R. L. Greene, K. Ramesha, J. Gopalakrishnan, J. Phys.: Condens. Matter 12, 965, (2000).
[9]   M. C. Viola, M. J. Martínez-lope, J. A. Alonso, P. Velasco, J. L. Martínze, J. C. Pedregosa, R. E. Carbonio, M. T. Fernández-Díaz, Chem. Mater. 14(2), (2002), 812.
[10]   S. Yu. Savrasov, D. Yu. Savrasov, Phys. Rev. B 46, 12181–12195 (1992)
[11]   S. Y. Savrasov, program LMTART for electronic structure calculations, Los Almos National Laboratory, 2004.
[12]   Glenn J. Martyna, Mark E. Tuckerman, J. Chem. Phys. 110, 2810 (1999).
[13]   S. Y. Savrasov, "FULL-POTENTIAL PROGRAM PACKAGE"LMTART 6.50" USER's MANUAL", New Jersey Institute of Technology, May 2, 2004
[14]   Vladimir I. Anisimovy, F. Aryasetiawanz, A. I. Lichtenstein, J. Phys.: Condens. Matter 9, (1997), 767.
[15]   S. L. Dudarev, G. A. Botton, S. Y. Savrasov, C. J. Humphreys, A. P. Sutton Phys. Rev. B 57, 1505 (1998).
[16]   X F Zhu, Q F Li, L F Chen, J. Phys.: Condens. Matter 20, 20075218, (2008).
[17]   Antonis Andriotis, R. Michael Sheetz, Madhu Menon, Phys. Rev. B 81, 245103, (2010).
[18]   Victor M. Goldschmidt, "Die Gesetze der Krystallochemie". Die Naturwissenschaften 21, (1926), 477.
[19]   M. W. Lufaso, P. M. Woodward, Acta. Cryst. B57, (2001), 725.
[20]   C. M. Bonilla, D. A. Landinez, J. Arbey, E. Vera Lopez, J. Roa-Rojas, Phys. B 398, (2007), 208.
[21]   M. Retuerto, J.A. Alonso, M. Garcia-Hernandez, M.J. Martinez-Lope, Solid State Commun. 139, (2006), 19.
[22]   W. Westerburg, O. Lang, C. Felser, W. Tremel, M. Waldeck, F. Renz, P. Gutlich, C. Ritterk, G. Jakob, Solid State Commun. 122, 3-4, (2002), 201.
[23]   A. Winkler, N. Narayanan, D. Mikhailova, K. G. Bramnik, H. Ehrenberg, H. Fuess, G. Vaitheeswaran, V. Kanchana, F. Wilhelm, A. Rogalev, A. Kolchinskaya, L. Alff, New J. Phys. 11, 073047, (2009).
[24]   R. Shaheen, J. Bashir, H. Rundlöf, A.R. Rennieb, Mater. Letts. 59, 18, (2005), 2296.
[25]   Song-Ho Byeon, Seoung-Soo Lee, John B. Parise, Patrick M. Woodward, Chem. Mater. 18 (16), (2006), 3873
[26]   http://www.unf.edu/~michael.lufaso/spuds/

[27]   A. K. Azad, S. A. Ivanov, S. G. Eriksson, H. Rundlof, J. Eriksen, R. Mathieu, P. Svedlindh, J. Magn. Magn. Mater. 237 (2001), 124.
[28]   T. S. Chan, J.-F. Lee, R. S. Liu, J. Phys.: Conference Series 190 (2009) 012095.
[29]   http://environmentalchemistry.com/yogi/periodic/ionicradius.html
[30]   Y. Suzuki, W.A. Sibley, O.H. El Bayoumi, T.M. Roberts, B. Bendow, Phys. Rev. B 35, 4472 – 4482, (1987).
[31]   R. Nistoraa, L. Andreicia, N. M. Avram, Acta Phys. Pol. 4, V. 116, (2009), 538.
[32]   J. B. Philipp, P. Majewski, L. Alff, R. Gross, T. Graf, M. S. Brandt, J. Simon, T. Walther, W. Mader, D. Topwal, D. D. Sarma, Phys. Rev. B 68, 144431, (2003).
[33]   J. Orna, L. Morellon, P.A. Algarabel, J.A. Pardo, C. Magen, M. Varela, S.J. Pennycook, J.M. De Teresa, M.R. Ibarra, J. Magn. Magn. Mater. 322, (2010), 1217.
[34]   Q. F. Li, X. F. Zhu, L. F. Chen, J. Phys.: Condens. Matter 20, 255230, (2008).
[35]   Hua Wu, Phys. Rev. B 64, 125126, (2001).
[36]   A. Arulraj, K. Ramesha, J. Gopalakrishnan, C. N. R. Rao, J. Solid State Chem. 155, 233, (2000).
[37]   Y. Moritomo, Sh. Xu, A. Machida, T. Akimoto, E. Nishibori, M. Takata, M. Sakata, Phys. Rev. B 61, R7827, (2000).
[38]   Horng-Tay Jeng, G. Y. Guo, Phys. Rev. B 67, 094438, (2003).
[39]   G. Vaitheeswaran, V. Kanchana, A.Delin, J. Phys.: Confer. Ser. 29 (2006), 50.
[40]   Tapas Kumar Mandal, Claudia Felser, Martha Greenblatt, Jürgen Kübler, Phys. Rev. B 78, 134431, (2008).
[41]   P. Majewski, S. Geprägs, A. Boger, M. Opel, A. Erb, R. Gross, G. Vaitheeswaran, V. Kanchana, A. Delin, F. Wilhelm, A. Rogalev, L. Alff, Phys. Rev. B 72, 132402, (2005).
[42]   H. Kato, T. Okuda, Y. Okimoto, Y. Tomioka, Y. Takenoya, A. Ohkubo, M. Kawasaki, Y. Tokura, Appl. Phys. Lett. 81, 328 (2002).
[43]   Electronic Structure: Basic Theory and Practical Methods, Richard M. Martin, Cambridge University Press, 2004.
[44]   C. Q. Tang, Y. Zhang, J. Dai, Solid State Commun. 133, (2005), 219.